Corresponding Author: Dr. Andrea Pirone,

Corresponding Author's Institution:

First Author: Andrea Pirone

Order of Authors: Andrea Pirone; Chiara Magliaro; Elisabetta Giannessi; Arti Ahluwalia

Abstract: Although the detailed structure and function of the claustrum remain enigmatic, its extensive reciprocal connection with the cortex suggests a role in the integration of multisensory information.Claustrum samples, obtained from necropsy of four dogs, were formalin fixed for paraffin embedding. Sections were either stained for morpho-histological analysis or immunostained for parvalbumin (PV). We focused on PV because it is a marker of the fast-spiking interneurons which have an important role in the information transmission and processing. Soma area, perimeter and circularity were considered as morphological parameters to quantitatively group the PV positive somata by k-means clustering.The histological investigation revealed a superior pyramidoid puddle and a posterior puddle characterized by a "cloud" of neurons in its dorso-lateral part. Immunostaining showed positive somata and fibers throughout the rostro-caudal extent of the dog claustrum, localized principally in the dorsal region. K-means clustering analysis enabled neuron classification according to size, identifying respectively big (radius =11.42±1.99 μm) and small (radius=6.33±1.08 μm) cells. No statistical differences in soma shape were observed. The topographical distribution of PV immunoreactivity suggests that the dog dorsal claustrum might be functionally related to the processing of visual inputs.Taken together our findings may help in the understanding the physiology of claustrum when compared with anatomical and functional data obtained in other species.

Pisa, December 2, 2014

To the Editor,
Journal of Chemical Neuroanatomy

Dear Editor,

please find enclosed herewith a manuscript titled "Parvalbumin expression in the claustrum of the dog. An immunohistochemical and topographical study with comparative notes on the structure of the nucleus", that I would like to submit to the *Journal of Chemical Neuroanatomy*. Considering the renewed and growing interest about this enigmatic structure (http://journal.frontiersin.org/ResearchTopic/1745) we decided to carry out a study in a species whose claustrum has not been investigated so far. The data reported in the manuscript are interesting, and I hope the reviewers will find them worthy.

As the corresponding author of the manuscript I declare that all the other authors fully agree with its content, and approve the text. I also declare that the manuscript has not been submitted elsewhere, and has never been published before in any form.

Sincerely yours,

Andrea Pirone
Department of Veterinary Sciences
University of Pisa
viale delle Piagge 2
56124 Pisa
ITALY
phone + 39.050.2216808
e-mail apirone@vet.unipi.it

Title:

Parvalbumin expression in the claustrum of the dog. An immunohistochemical and topographical study with comparative notes on the structure of the nucleus.

Authors:

Andrea Pirone[1], Chiara Magliaro[2], Elisabetta Giannessi[1], Arti Ahluwalia[2]

[1] Department of Veterinary Sciences, University of Pisa, Pisa, Italy

[2] Research Center "E. Piaggio", Faculty of Engineering, University of Pisa, Pisa, Italy

Corresponding author: Andrea Pirone, Department of Veterinary Sciences, University of Pisa, 56124 Pisa, Italy, andrea.pirone@unipi.it, phone + 39.050.2216808

Running headline: Parvalbumin in the dog claustrum

Key words: claustrum; dog; parvalbumin; puddle

Abstract

Although the detailed structure and function of the claustrum remain enigmatic, its extensive reciprocal connection with the cortex suggests a role in the integration of multisensory information. Claustrum samples, obtained from necropsy of four dogs, were formalin fixed for paraffin embedding. Sections were either stained for morpho-histological analysis or immunostained for parvalbumin (PV). We focused on PV because it is a marker of the fast-spiking interneurons which have an important role in the information transmission and processing. Soma area, perimeter and circularity were considered as morphological parameters to quantitatively group the PV positive somata by k-means clustering.

The histological investigation revealed a superior pyramidoid puddle and a posterior puddle characterized by a "cloud" of neurons in its dorso-lateral part. Immunostaining showed positive somata and fibers throughout the rostro-caudal extent of the dog claustrum, localized principally in the dorsal region. K-means clustering analysis enabled neuron classification according to size, identifying respectively big (radius =11.42 ± 1.99 µm) and small (radius=6.33 ± 1.08 µm) cells. No statistical differences in soma shape were observed. The topographical distribution of PV immunoreactivity suggests that the dog dorsal claustrum might be functionally related to the processing of visual inputs.

Taken together our findings may help in the understanding the physiology of claustrum when compared with anatomical and functional data obtained in other species.

1. Introduction

The claustrum is a subcortical telencephalic structure present in all the placental mammals investigated so far (Kowianski et al., 1999). Due to its modest size, intricate shape and deep internal location, its anatomy, physiology and ontogenesis is still a matter of debate (Edelstein and Denaro, 2004, Pirone et al., 2012, Mathur, 2014). It has an extensive afferent and efferent network with the cortex, with a special relationship to the visual cortex in the cat (Olson and Graybiel, 1980, Minciacchi et al., 1995) and monkey (Remedios et al., 2010), consequently it has been hypothesized that this structure might be a nervous center where different cortical information are processed and integrated (Crick and Koch, 2005). Crick and Koch (2005) refer to the claustrum as "a conductor coordinating a group of players in the orchestra, the various cortical regions". In line with this view, Smythies et al. (2012, 2014) described the claustrum interneurons as an "interactive gap-junction syncytium".

Nevertheless, a recent anatomical study including various species depicted the claustrum as an irregular structure with many isolated cells islands observed in cetaceans (Baizer et al., 2014). According to these discontinuities the authors argued against the postulated role of the claustrum as a conductor.

The claustral interneurons, as in the cortex (Druga, 2009), seem to play a crucial role in the inhibitory circuits providing a substrate for local information processing (Crick and Koch, 2005).

Calcium-binding proteins (CBps) (calretinin CR, calbindin CB and parvalbumin PV) are considered markers of three non-ovarlapping interneuronal populations (Druga, 2009, Barinka and Druga, 2010). Moreover, a recent study indicates that cortical interneurons can also be classified by their expression of PV, somatostatin, and vasointestinal peptide (Xu et al., 2010).

PV is a marker of a specific class of interneurons, the category of fast-spiking neurons, involved in the generation of gamma oscillations which have an important role in the transmission of information between cortical and hippocampal areas (Buzsaki et al., 1983; Whittington et al., 1995; Tamas et al., 2000; Salinas and Sejnowski, 2001; Bartos et al., 2007; Freund and Katona, 2007; Gonzalez-Burgos and Lewis, 2008; Roopun et al., 2008; Cardin et al., 2009; Uhlhaas and Singer, 2010).

The presence of PV-immunoreactive (ir) interneurons, with gap junctions along their dendrites, was described in the cerebral cortex sopragranular layer (Fukuda, 2007). Gap junctions, thus electrical synapses, are regarded as an important factor of synchronous activity (Galarreta and Hestrin, 2001, Hestrin and Galarreta, 2005). Interestingly, a decrease of PV-ir interneurons seems to result in a reduction in coordinated neuronal activity during task performance in a rat model of schizophrenia

(Lodge et al., 2009). Moreover, a decrease of PV-ir neurons in the central nervous system of patients with Alzheimer's disease has been observed (Satoh et al., 1991). Dogs show many neurological disorders which phenotypically resemble human diseases, thus this species can be used as a good model for investigating the cellular mechanism of pathologies in the human brain (Colle et al., 2000, Head et al., 2000, Rofina et al., 2003, Skoumalova et al., 2003).

In this study we investigated the topographic distribution and morphology of PV-ir neurons in the dog claustrum. Moreover, in the light of recent anatomical studies (Baizer et al., 2014, Johnson et al., 2014) we analyzed the histological features of this enigmatic structure. Although many immunohistochemical studies have shown the presence of PV in the claustrum of different animals (Real et al., 2003; Wojcik et al., 2004; Rahman and Baizer, 2007; Cozzi et al., 2014, Pirone et al., 2014), and a recent detailed study also describes the distribution of PV in the human claustrum (Hinova-Palova et al., 2014), to the best of our knowledge no data on the presence of this protein in the dog claustrum have been reported.

2. Material and methods

2.1 Animals and tissue sampling

Claustrum samples were obtained from necropsy of four dogs referred to the Department of Veterinary Science of the University of Pisa for post-mortem examination. Anamnestic data and notes are reported in (Table 1). CNS abnormalities were excluded by histopathological examination. The brains, extracted within 6 h of death for routine diagnostic scopes, were cut in coronal slabs (0.5 cm thick) fixed by immersion in buffered formalin and processed for paraffin embedding.

Since archival samples were used, Institutional Animal Care and Use Committee approval was not required. Use of archival samples is encouraged by the EU Directive 2010/63/ of 22 September 2010 on the protection of animals used for scientific purposes.

No.	Breed	Age	Sex	Cause of death
1	Dachshund	11	female	intra-abdominal hemorrhage
2	Fox Terrier	12	male	peritonitis
3	Mixed-breed	4	male	trauma
4	Mixed-breed	9	male	heart failure

Table 1. Details of the sampled dogs.

2.2 Histology

Each slab containing both cerebral hemispheres was cut in two halves following the sagittal median plane along the longitudinal fissure and embedded in serial paraffin blocks. Transverse sections cut with a microtome (5 µm) from the left hemisphere were stained with Luxol Fast Blue (for myelin) while sections from the right hemisphere were used for Nissl staining. The claustrum and the adjoining structures were examined in accordance with a sterotaxic atlas (Palazzi, 2011).

2.3 Immunohistochemistry

Immunohistochemistry was performed on serial sections belonging to the left hemisphere using a mouse monoclonal anti PV antibody (1:5000, cod. no. 235, lot. no.10-11 F, Swant, Bellinzona, Switzerland). Epitope retrieval was carried out at120 °C in a pressure cooker for 5 min with a Tris/EDTA buffer pH 9.0. Sections were pretreated in 1% H_2O_2 (in 0.1M PBS, pH 7.4, 10 min) to quench endogenous peroxidase activity, then rinsed with 0.05% tween-20 detergent (in 0.1M PBS, 3 x 10 min.), and blocked with 5% goat normal serum (s-1000, Vector) (in 0.1M PBS, 1h). Sections were incubated overnight at 4 °C in a solution containing the mouse anti-PV, 2% goat normal

serum, 0.05% triton X-100 (in 0.1M PBS). Subsequently they were rinsed in 0.1M PBS, (3 x 10 min), followed by incubation with a biotinylated goat anti-mouse immunoglobulin (BA-9200, Vector Labs, Burlingame, CA), diluted 1:300 in PBS. Sections were again rinsed in 0.1M PBS, for 3 x 10 min. Staining was visualized by incubating the sections in diaminobenzidine (DAB) (sk-4105, Vector, Burlingame, CA) solution.

The specificity of the immunohistochemical staining was tested in repeated trials as follows: substitution of either the primary antibody, or anti-mouse IgG, or the ABC complex by PBS or non-immune serum. Under these conditions the staining was abolished.

Whole slide images were acquired with Aperio Scanscope CS (Leica Biosystems Imaging, Inc. USA). The microphotographs were taken with a light microscope (Leitz Diaplan,Wetzlar, Germany) connected to a PC via a Nikon digital system (Digital Sight DS-U1, NIS-Elements BR-4.13.00 software).

2.4 Image acquisition and processing

As neurons have a three dimensional structure it is not possible to track all the neurites constituting a neuron on a single histological slice. For this reason, rather than tracing and quantifying neurites, we quantified shape parameters of 200 PV stained somata for each of the 4 dogs, in order to classify neurons according to soma shape and size. All images were acquired with the light microscope using a 25x objective and processed with the Nikon NIS-Elements BR-4.13.00 software which allows the measurement of different morphological features. In particular, the parameters extracted are soma area and perimeter as benchmarks of size, and circularity (4π x AREA/(PERIMETER)2)) as shape descriptor. In order to classify neuron somata, the dataset obtained was analysed using the k-means clustering algorithm (Arthur and Vassilvitskii, 2007). This technique enables data grouping using an iterative algorithm that assigns objects to clusters minimizing the sum of distances from each object to its cluster centroid.

To assess the goodness of the clustering, statistical analysis was performed considering the data extracted from the population obtained.

3 Results

In all the examined dogs claustrum four subsequent rostro-caudal levels were considered for histological and immunohistochemical analysis (Figure 1).

3.1 Histology

As showed by the histological stains (Figures 2B-5B) the shape of the dog claustrum changes with rostro-caudal level. In particular, in our most rostral section the dorso-lateral extension of the claustrum is formed by a thin lamina which stretches out into the white matter dorsal parallel to the cortex; the lamina widen in the ventral direction towards the rhinal sulcus (Figure 2B). At about the centre of the insular claustrum a prominent dorsal enlargement and a ventral "banana"-like region, linked by a thin stem, were found (Figure 3B). The ventral region seems to reach the piryform cortex. The dorsal enlargement fills the space left by the putamen. At thalamic level (Figure 4B), the enlargement appears to be smaller with a pyramidoid shape descending with a thin stem towards the amygdaloid nucleus. In general, the accurate estimation of the ventromedial boundary of the claustrum was difficult.

Proceeding caudalward, the claustrum was found to have an elliptic shape. Dorso-laterally to the elliptic shaped claustrum, a "cloud" of neurons was noted (Figures 5B, 7C, 7D). In Nissl sections each soma in the "cloud" was in close contact with at least two satellite oligodendrocytes (Figure 7 A, C); with respect to those of the claustrum (Figure 7 E, C) they displayed a lower density. Moreover, unlike the claustrum neurons (Figure 7 D, F) they were embedded in a dense meshwork of thick myelinated fibers (Figure 7B, D).

Luxol Fast Blue stained sections (Figure 2B-5B, left side) depicted the dog claustrum as a lightly myelinated structure; this was particularly evident if compared to the external and the extreme capsules (Figure 8B). The latter was generally thinner than the external capsule and in Nissl stained sections presented numerous cells (Figure 8A).

3.2 Immunohistochemistry

Immunostaining revealed PV-ir neurons and fibers throughout the dog claustrum with a non-uniform distribution pattern. In the immunostained sections the claustrum was clearly outlined against the white matter. Chartings in the schematic drawings (Figures 2A-5A right side) represent the relative density of the PV-ir cells. In the rostral-most section the number of positive cells increased moving ventrally (Figure 2A). In particular, in the dorsal part where the claustrum is a

thin lamina, bent over the cortex, we found only few elongated somata with their main axis parallel to the borders of the structure.

In the central region of the claustrum (Figures 3A-4A) we noted a different distribution pattern. Here, the immunostained cells and fibers were clearly concentrated in the dorsal expanded zone decreasing from a dorsal to ventral perspective. In the thin stem which links the dorsal enlargement to the ventral part labeled cells and fibers were rare (Figure 4 A, C, D).

In our caudal most sections (Figure 5) the claustrum was elliptically shaped; PV-ir neurons and fibers were homogeneously distributed. Dorso-laterally we identified a cloud of neurons formerly described in the histological section (Figure 5B), where immunostained cells and fibers (Figure 5 C, D) showed a lower density compared to the claustrum (Figure 5 C, E).

Scarce PV-ir somata and fibers were also spotted in both the external and the extreme capsule (Fig. 6).

As a rule the PV-ir somata were darkly stained. Their shape appeared to be fusiform (Figure 2D, 3D), round (Figure 3D), triangular (Figure 3D), pear-like (Figure 3D) or polygonal (Figures 2D, 5E). The labeled neuropil displayed numerous longitudinal positive fibers and puncta. The latter surrounded the claustrum non-PV-ir somata (Figure 2D, 5E, 6C).

3.3 Morphometric analysis

Image analysis enables the identification of the main morphological features of neuron somata. A k-means clustering was performed on the morphometric dataset so as to group neurons on the basis of the measured variables. To identify the right number of clusters and establish how well-separated the groups are, we measure how close each point in one cluster is to points in the other clusters through the so-called silhouette value. In our case, two clusters were identified. In fact, the silhouette plot (Fig. 9), which represents each neuron as a pixel-thick horizontal line with a length corresponding to its silhouette value, shows that most points in both clusters have a large silhouette value, greater than 0.8, indicating that those points are well-separated from neighboring clusters. Only few very small neuron somata are badly matched to the others belonging to the same cluster (silhouette value < 0). The two groups obtained are statistically different in term of soma size. In fact, on the basis of the soma features extracted, the k-means analysis allows the classification of neurons by soma radius: in one group the soma are big (11.42±1.99 µm), while the other they are small (6.33±1.08 µm).

No difference were observed in soma shape, indeed the circularity value for cluster 1 was 0.70 ± 0.14 while for cluster 2 was 0.75 ± 0.12.

T-test analysis confirms the results obtained. In fact, as regards soma radius, the difference in the population means are significantly different (p<0.05), while no difference was observed regarding soma circularity.

4. Discussion

4.1 Histology

Data on the dog claustrum histology are scanty and rely on two works (Miodonski, 1975, Maciejewska et al., 1994). Broadly, our findings are in agreement with their reports, indeed we also describe a dorsal and a ventral claustrum connected by a thin stem.

On the other hand, in the most caudal part we observed an elliptic-shaped enlargement of the claustrum with a "cloud" of neurons in its dorso-lateral part. A recent anatomical study has introduced the notion of "claustral puddle" as an enlargement formed by claustral cells that filled the empty spaces left by the adjoining structures (Johnson et al., 2014). In the dog we identified a superior pyramidoid puddle and a posterior puddle. This scheme is in accordance with reported observations in the red fox (Johnson et al., 2014). However, no literature data refer to the cloud of neurons we observed dorso-laterally with respect to the posterior puddle. According to our findings we can hypothesize either that this structure is not part of the claustrum or that it is a part of the posterior claustrum. This latter hypothesis might be in line with the discontinuities described by Baizer et al. (2014) in the claustrum of animals with large brains although in the histological sections we did not find a clear discontinuity between the claustrum and the cloud of neurons. However, following the former hypothesis, these neurons might represent the posterior extent of the insular pocket. Further investigations are needed to clarify the nature of this cluster of neurons.

Nissl and Luxol Fast Blue stained sections highlighted the boundaries between the claustrum and either the extreme capsule or the external capsule. The extreme capsule separates the claustrum from the insular cortex; the relationship between these two latter structures is generally discussed to hypothesize the origin of claustrum. The ontogenesis of the claustrum is indeed still a matter of debate. Three main theories exist: according to the pallial theory, the claustrum is considered a derivative of insular cortex. A second theory depicts the claustrum as derived from the basal ganglia. The third theory, or hybrid theory, supports the hypothesis that the claustrum has both a pallial and a sub-pallial derivation (Edelstein and Denaro, 2004). Some authors described the claustrum as a part of the insular layer VI (Meynert, 1868, Brodmann, 1909). In addition, histological findings in Microcebus murinus depicted the claustrum as an extra layer of the insula (Park et al., 2012). In our Nissl and Luxol Fast Blue stained sections the extreme capsule was very thin so that the insula and the claustrum were hardly separate from each other. Besides, in the extreme capsule several neurons were observed; this evidence suggests, in agreement with the pallial theory, that the claustrum and the insula could share a common origin, at least in the dog.

4.2 Immunohistochemistry

4.2.1 PV-ir neuron distribution

To the best of our knowledge, our findings are the first to show the topographical distribution of PV-ir neurons in the dog claustrum. The positive somata and fibers are distributed throughout the rostro-caudal extent of the dog claustrum. With the exception of the rostral most part, the labeled elements were mainly localized in the dorsal region, in particular in the superior pyramidoid puddle and in the posterior puddle. The immunostaining technique we employed (paraffin sections of 5 µm) did not allow us to describe the dendritic arborization.

The major difference we found between the present study and those of other authors concerns the topographical distribution of PV-ir neurons. In the dog, immunostained somata were clearly concentrated in the dorsal pyramidoid puddle while only a small-to-modest number of positive neurons were noted in the ventral part. The exception to this scheme was the most rostral part of the claustrum, where the distribution pattern was the opposite. Real et al. (2003), who investigated CBPs expression in the dorsal and ventral (endopiriform nucleus, ED) division of the mouse claustrum, showed that PV-ir cells were more numerous in the dorsal division than in the ventral. Moreover, in the rabbit the PV immunoreactivity in the ED was lower than that observed in the dorsal claustrum (Wojcik et al., 2004). In addition, in human and chimpanzee PV immunostained cells were more concentrated in the central and in the ventral part (Pirone et al., 2014, Hinova-Palova et al., 2014). However, a comparison of the PV immunoreactivity distribution among different species is difficult because of species-specific variations in PV-ir labeling (Baimbridge et al., 1992).

We observed non-PV-ir neurons surrounded by immunoreactive terminals. This suggested that many neurons make extensive intraclaustral connections corroborating the theory of a structure where cortical information is processed and integrated (Crick and Koch, 2005).

4.2.2 PV-ir somata Morphometrics

The variability of PV-ir somata shape is consistent with that already reported in other species such as: mouse (Real et al., 2003), rat (Celio, 1990), rabbit (Wojcik et al., 2004), cat (Rahman and Baizer, 2007, Hinova-Palova et al., 2007), monkey (Reynhout and Baizer, 1999), chimpanzee (Pirone et al., 2014) and human (Pirone et al., 2014, Hinova-Palova et al., 2014). In particular, the shapes of PV-ir somata we described in the dog are analogous to the findings reported in the cat

claustrum (Rahman and Baizer, 2007) which, among the above mentioned species, is phylogenetically closer to the dog.

To classify somata on the basis of their shape and size, we used statistical methods to cluster the data acquired from image analysis. This method is more objective than the commonly used method of arbitrarily defining a series of radius limits to define cell size. The main morphological features of the immunostained somata regarding both size and shape are summarized in Figure 9. K-means clustering analysis identified two well-separated groups, cluster 1's population was about 2.4x times that of cluster 2.

A recent study in the human claustrum classified PV-ir neurons in spiny and aspiny each further arbitrarily divided according to the soma radius in large, medium and small (Hinova-Palova et al., 2014). Similar findings on soma radius have been described in the cat claustrum (Rahman and Baizer, 2007; Hinova-Palova et al., 2007). In particular, the clusters we found according to the radius were in line with the categories of small (13-15 µm in diameter) and medium (15-20 µm up to 25 µm in diameter) somata observed by Hinova-Palova et al. (2007).

LeVay and Sherk (1981) using Golgi preparations described in the cat visual claustrum large spiny (15-29 µm in diameter) and small aspiny (10-15 µm in diameter) neurons.

Although it is difficult to compare an immunohistochemical study to a Golgi study, it is possible to note some similar aspects. The radius values of the two cluster we found was in agreement with those reported in the cat visual claustrum (LeVay and Sherk, 1981). Moreover, these authors described the large spiny as the most frequent type.. According to these findings we can speculate that in the dog claustrum most likely the PV-ir soma of the cluster 1 are spiny neurons while those of the cluster 2 are probably small aspiny neurons.

4.3 Comparisons with other species

Many anatomical studies have demonstrated reciprocal and topographically organized connections between the claustrum and the cerebral cortex (Mathur, 2014, Edelstein and Denaro, 2004). In the human and chimpanzee the dorsal claustrum maintains the extensive relationship with the somatosensory and with the auditory cortical areas demonstrated in the Rhesus monkey (Minciacchi et al., 1991, Remedios et al., 2010). Moreover, in the macaque monkey the segregation of the visual modality in the ventro-caudal claustrum was observed (Remedios et al., 2010, Gattass et al., 2014). Differently, in the cat the posterior-dorsal claustrum has been defined as the visual claustrum (LeVay and Sherk, 1981).

Regarding the visual connection, we can postulate for the dog claustrum a pattern similar to the cat. This is consistent with the presence of a dorsal pyramidoid puddle both in the dog (present study) and in the cat (LeVay and Sherk, 1981, Rahman and Baizer, 2007). It remains to be established whether the higher density of PV-ir neurons in the dorsal claustrum, observed in the present study, is functionally related to the processing of visual (rather than somatosensory and auditory) information. However, some evidence indicates that PV-ir interneurons were targets of feedforward and feedback connections among areas of the rat visual cortex (Gonchar and Burkhalter, 2003), in rat thalamocortical pathway (Staiger et al., 1996) and in connections from layer 3 to 4 of cat visual cortex (Thomson et al., 2002). It has been suggested that the preferred target of these connections seem to be PV expressing interneurons rather than other types of interneurons (Gonchar and Burkhalter, 2003). Based on the studies mentioned above and on our findings, we can speculate that the dorsal pyramidoid puddle could also be reciprocally connected with the visual cortex.

Taken together our findings related to the histology and topography of the PV-ir neurons may help in the understanding the physiology of claustrum when compared with other anatomical and functional data obtained in other species. Further data are needed to better characterize the populations of interneurons of the canine claustrum as well as the circuitry it contributes to.

References

Arthur, D., Vassilvitskii, S., 2007. k-means++: The advantages of careful seeding. In Proceedings of the eighteenth annual ACM-SIAM symposium on Discrete algorithms), pp. 1027-1035. Society for Industrial and Applied Mathematics.

Baimbridge, K.G., Celio, M.R., Rogers, J.H., 1992. Calcium-binding proteins in the nervous system. Trends Neurosci. 15, 303-8.

Baizer, J.S., Sherwood, C.C., Noonan, M., Hof, P.R., 2014. Comparative organization of the claustrum: what does structure tell us about function? Front. Syst. Neurosci. 8, 117.

Barinka, F., Druga, R., 2010. Calretinin expression in the mammalian neocortex: a review. Physiol. Res. 59, 665-77.

Bartos, M., Vida, I., Jonas, P., 2007. Synaptic mechanisms of synchronized gamma oscillations in inhibitory interneuron networks. Nat. Rev. Neurosci. 8, 45-56.

Brodmann, K., 1909. Vergleichende Lokalisationslehre der Grosshirnrinde in ihren Prinzipien dargestellt auf Grund des Zellenbaues, Barth.

Buzsaki, G., Leung, L.W., Vanderwolf, C.H., 1983. Cellular bases of hippocampal EEG in the behaving rat. Brain Res. 287, 139-71.

Cardin, J.A., Carlen, M., Meletis, K., Knoblich, U., Zhang, F., Deisseroth, K., Tsai, L.-H., Moore, C.I., 2009. Driving fast-spiking cells induces gamma rhythm and controls sensory responses. Nature 459, 663-7.

Celio, M.R., 1990. Calbindin D-28k and parvalbumin in the rat nervous system. Neuroscience 35, 375-475.

Colle, M.A., Hauw, J.J., Crespeau, F., Uchiharaa, T., Akiyamaf, H., Checlerg, F., Pageath, .P, Duykaerts, C., 2000. Vascular and parenchymal Aβ deposition in the aging dog: correlation with behavior. Neurobiol. Aging 21, 695-704.

Cozzi, B., Roncon, G., Granato, A., Giurisato, M., M. Castagna, Peruffo, A., Panin, M., Ballarin, C., Montelli, S., Pirone, A., 2014. The claustrum of the bottlenose dolphin *Tursiops truncatus* (Montagu 1821). Front. Syst. Neurosci. 8, 42.

Crick, F.C., Koch, C., 2005. What is the function of the claustrum? Philos. Trans. R. Soc. Lond. B. Biol. Sci. 360, 1271-9.

Druga, R., 2009. Neocortical inhibitory system. Folia Biol. (Praha) 55, 201-17.

Edelstein, L.R., Denaro, F.J., 2004. The claustrum: a historical review of its anatomy, physiology, cytochemistry and functional significance. Cell Mol. Biol. (Noisy-le-grand) 50, 675-702.

Freund, T.F., Katona, I., 2007. Perisomatic inhibition. Neuron 56, 33-42.

Fukuda, T., 2007. Structural organization of the gap junction network in the cerebral cortex. Neuroscientist 13, 199-207.

Galarreta, M., Hestrin, S., 2001. Spike transmission and synchrony detection in networks of GABAergic interneurons. Science 292, 2295-9.

Gattass, R., Soares, J.G., Desimone, R., Ungerleider, L.G., 2014. Connectional subdivision of the claustrum: two visuotopic subdivisions in the macaque. Front. Syst. Neurosci. 8, 63.

Gonchar, Y., Burkhalter, A., 2003. Distinct GABAergic targets of feedforward and feedback connections between lower and higher areas of rat visual cortex. J. Neurosci. 23, 10904-12.

Gonzalez-Burgos, G., Lewis, D.A., 2008. GABA neurons and the mechanisms of network oscillations: implications for understanding cortical dysfunction in schizophrenia. Schizophr. Bull. 34, 944-61.

Head, E., Thornton, P.L., Tong, L., Cotman, C.W., 2000. Initiation and propagation of molecular cascades in human brain aging: insight from the canine model to promote successful aging. Prog. Neuropsychopharmacol. Biol. Psychiatry 24, 777-86.

Hestrin, S., Galarreta, M., 2005. Electrical synapses define networks of neocortical GABAergic neurons. Trends Neurosci. 28, 304-9.

Hinova-Palova, D.V., Edelstein, L., Paloff, A.M., Hristovc, S., Papantcheva, V.G., Ovtscharoff, W.A., 2007. Parvalbumin in the cat claustrum: Ultrastructure, distribution and functional implications. Acta Histochem. 109, 61-77.

Hinova-Palova, D.V., Edelstein, L., Landzhov, B.V., Braak, E., Malinova, L.G., Minkov, M., Paloff, A., Ovtscharoff, W., 2014. Parvalbumin-immunoreactive neurons in the human claustrum. Brain Struct. Funct. 219, 1813-30.

Johnson, J.I., Fenske, B.A., Jaswa, A.S., Morris, J.A., 2014. Exploitation of puddles for breakthroughs in claustrum research. Front. Syst. Neurosci. 8, 78.

Kowianski, P., Dziewiatkowski, J., Kowianska, J., Morys, J., 1999. Comparative anatomy of the claustrum in selected species: A morphometric analysis. Brain Behav. Evol. 53, 44-54.

LeVay, S., Sherk, H., 1981. The visual claustrum of the cat. I. Structure and connections. J. Neurosci. 1, 956-80.

Lodge, D.J., Behrens, M.M., Grace, A.A., 2009. A loss of parvalbumin-containing interneurons is associated with diminished oscillatory activity in an animal model of schizophrenia. J. Neurosci. 29, 2344-54.

Maciejewska, B., Morys, J., Berdel, B., Narkiewicz, O., 1994. Insular claustrum of the dog--a morphometric investigation of cellular structure. Folia Morphol. (Warsz) 53, 209-19.

Mathur, B.N., 2014. The claustrum in review. Front. Syst. Neurosci. 8, 48.

Meynert, T., 1868. Neue Untersuchungen über den Bau der Grosshirnrinde und ihre örtliche Verschiedenheiten. Alleg. Wien. Medizin. Ztg. 13, 419-428.

Minciacchi, D., Granato, A., Antonini, A., Tassinari, G., Santarelli, M., Zanolli, L., Macchi, G., 1995. Mapping subcortical extrarelay afferents onto primary somatosensory and visual areas in cats. J. Comp. Neurol. 362, 46-70.

Minciacchi, D., Granato, A., Barbaresi, P., 1991. Organization of claustro-cortical projections to the primary somatosensory area of primates. Brain Res. 553, 309-12.

Miodonski, R., 1975. The claustrum in the dog brain. Acta Anat. (Basel) 91, 409-22.

Olson, C.R., Graybiel, A.M., 1980. Sensory maps in the claustrum of the cat. Nature 288, 479-81.

Palazzi, X., 2011. The Beagle Brain in Stereotaxic Coordinates. Springer.

Park, S., Tyszka, J.M., Allman, J.M., 2012. The Claustrum and Insula in Microcebus murinus: A High Resolution Diffusion Imaging Study. Front Neuroanat. 6, 21.

Pirone, A., Castagna, M., Granato, A., Peruffo, A., Quilici, F., Cavicchioli, L., Piano, I., Lenzi, C., Cozzi, B., 2014. Expression of calcium-binding proteins and selected neuropeptides in the human, chimpanzee, and crab-eating macaque claustrum. Front. Syst. Neurosci. 8, 99.

Pirone, A., Cozzi, B., Edelstein, L., Peruffo, A., Lenzi, C.,Quilici, F., Antonini, R., Castagna, M., 2012. Topography of Gng2- and NetrinG2-expression suggests an insular origin of the human claustrum. PLoS One 7, e44745.

Rahman, F.E., Baizer, J.S., 2007. Neurochemically defined cell types in the claustrum of the cat. Brain Res. 1159, 94-111.

Real, M.A., Davila, J.C., Guirado, S., 2003. Expression of calcium-binding proteins in the mouse claustrum. J. Chem. Neuroanat. 25, 151-60.

Remedios, R., Logothetis, N.K., Kayser, C., 2010. Unimodal responses prevail within the multisensory claustrum. J. Neurosci. 30, 12902-7.

Reynhout, K., Baizer, J.S., 1999. Immunoreactivity for calcium-binding proteins in the claustrum of the monkey. Anat. Embryol. (Berl) 199, 75-83.

Rofina, J., van Andel, I., van Ederen, A.M., Papaioannou, N., Yamaguchi, H., Gruys, E., 2003. Canine counterpart of senile dementia of the Alzheimer type: amyloid plaques near capillaries but lack of spatial relationship with activated microglia and macrophages. Amyloid 10, 86-96.

Roopun, A.K., Cunningham, M.O., Racca, C., Alter, K., Traub, R.D., Whittington, M.A., 2008. Region-specific changes in gamma and beta2 rhythms in NMDA receptor dysfunction models of schizophrenia. Schizophr. Bull. 34, 962-73.

Salinas, E., Sejnowski, T.J., 2001. Correlated neuronal activity and the flow of neural information. Nat. Rev. Neurosci. 2, 539-50.

Satoh, J., Tabira, T., Sano, M., Nakayama, H., Tateishi, J., 1991. Parvalbumin-immunoreactive neurons in the human central nervous system are decreased in Alzheimer's disease. Acta Neuropathol. 81, 388-95.

Skoumalova ,A., Rofina, J., Schwippelova, Z., Gruys, E., Wilhelm, J., 2003. The role of free radicals in canine counterpart of senile dementia of the Alzheimer type. Exp. Gerontol. 38, 711-9.

Smythies, J., Edelstein, L., Ramachandran, V., 2012. Hypotheses relating to the function of the claustrum. Front. Integr. Neurosci. 6, 53.

Smythies, J., Edelstein, L., Ramachandran, V., 2014. Hypotheses relating to the function of the claustrum II: does the claustrum use frequency codes? Front. Integr. Neurosci. 8, 7.

Staiger, J.F., Zilles, K., Freund, T.F., 1996. Distribution of GABAergic elements postsynaptic to ventroposteromedial thalamic projections in layer IV of rat barrel cortex. Eur. J. Neurosci. 8, 2273-85.

Tamas, G., Buhl, E.H., Lorincz, A., Somogyi, P., 2000. Proximally targeted GABAergic synapses and gap junctions synchronize cortical interneurons. Nat. Neurosci. 3, 366-71.

Thomson, A.M., West, D.C., Wang, Y., Bannister, A.P. 2002. Synaptic connections and small circuits involving excitatory and inhibitory neurons in layers 2-5 of adult rat and cat neocortex: triple intracellular recordings and biocytin labelling in vitro. Cereb. Cortex 12, 936-53.

Uhlhaas, P.J., Singer, W., 2010. Abnormal neural oscillations and synchrony in schizophrenia. Nat. Rev. Neurosci. 11, 100-13.

Whittington, M.A., Traub, R.D., Jefferys, J.G., 1995. Synchronized oscillations in interneuron networks driven by metabotropic glutamate receptor activation. Nature 373, 612-5.

Wojcik, S., Dziewiatkowski, J., Spodnik, E., Ludkiewicz, B., Domaradzka-Pytel, B., Kowiañski, P., Moryœ, J., 2004. Analysis of calcium binding protein immunoreactivity in the claustrum and the endopiriform nucleus of the rabbit. Acta Neurobiol. Exp. (Wars) 64, 449-60.

Xu, X., Roby, K.D., Callaway, E.M., 2010. Immunochemical characterization of inhibitory mouse cortical neurons: three chemically distinct classes of inhibitory cells. J. Comp. Neurol. 518, 389-404.

FIGURE LEGENDS

Figure 1. Photographs of macroscopic coronal sections of the canine brain showing the four subsequent rostro-caudal levels considered for histological description and immunohistochemical characterization of PV-ir neurons.

Figure 2. Microphotographs of immunohistochemical and histological staining of coronal brain sections. (A) Low magnification image (left side) of the PV-ir distribution in the left hemisphere including the claustrum; schematic draw (right side) with charting representing the relative density of the PV labeled somata (red dots) in the claustrum. (B) Low magnification image of a Luxol Fast Blue (left side) and Nissl (right side) stained sections. (C) Detail of A and (D) detail of C showing PV-ir neurons in the ventral claustrum. Empty arrow = polygonal soma; dashed arrow = fusiform soma; arrow = non-PV-ir soma surrounded by positive terminals. Cd, caudate nucleus; Cl, claustrum; ic, insular cortex; Rhf, rhinal fissure. Scale bars: A, B = 1 mm; C = 100 μm, D = 20 μm.

Figure 3. Microphotographs of immunohistochemical and histological staining of coronal brain sections. (A) Low magnification image (left side) of the PV-ir distribution in the left hemisphere; schematic draw (right side) with charting representing the relative density of the PV labeled somata (red dots) in the claustrum. (B) Low magnification image of a Luxol Fast Blue (left side) and Nissl (right side) stained sections. (C) Detail of A and (D) detail of C showing PV stained neurons in the dorsal claustrum. Empty arrow, triangular soma; dashed arrow, round soma; arrow, fusiform soma; arrow head, pear-like soma. Cd, caudate nucleus; Cl, claustrum; ic, insular cortex; LPy, pyriform lobe; Pu, putamen. Scale bars: A, B = 1 mm; C = 100 μm, D = 20 μm.

Figure 4. Microphotographs of immunohistochemical and histological staining of coronal brain sections.. (A) Low magnification image (left side) of the PV-ir distribution in the left hemisphere; schematic draw (right side) with charting representing the relative density of the PV labeled somata (red dots) in the claustrum. (B) Low magnification image of a Luxol Fast Blue (left side) and Nissl (right side) stained sections. (C) Detail of A and (D) detail of C showing PV stained neurons in the central claustrum. CA, hippocampus; Cl, claustrum; ic, insular cortex; PLVN, posterolateral ventral thalamic nucleus; Pu, putamen. Scale bars: A, B = 1 mm; C = 100 μm, D = 20 μm.

Figure 5. Microphotographs of immunohistochemical and histological staining of coronal brain sections. (A) Low magnification image (left side) of the PV-ir distribution in the left hemisphere; schematic draw (right side) with charting representing the relative density of the PV labeled somata (red dots) in the claustrum and in the adjoining region. (B) Low magnification image of a Luxol Fast Blue (left side) and Nissl (right side) stained sections. (C) Detail of A, (D) and (E) details of C showing PV stained neurons in the claustrum (E) and in the adjoining region (D). Empty arrow,

polygonal soma; arrow, non-PV-ir soma surrounded by positive terminals. CA, hippocampus; Cl, claustrum; DLGe, dorso-lateral geniculus; LGe, lateral geniculus; MGe, medial geniculus; SN, *substantia nigra*; ZI, *zona incerta*. Scale bars: A, B = 1 mm; C = 100 μm, D = 20 μm.

Figure 6. Photomicrographs of immunostained sections focusing at the capsules (external and extreme). (A) high magnification image (detail of B) focusing at the boundary (black line) between claustrum and the external capsule; (B) low magnification image including the claustrum and adjoining structures; (C) high magnification image (detail of B) focusing at the boundary (black line) between claustrum and the extreme capsule. Arrow, non-PV-ir soma surrounded by positive terminals. Cl, claustrum; Ex, external capsule; Ext, extreme capsule; Ic, insular cortex. Scale bars: B = 200 μm; A, C = 20 μm.

Figure 7. Histological characterization of the posterior claustrum puddle dorsolaterally flanked by a cluster of neurons ("cloud"). (A) Photomicrograph (detail of C) showing the presence of multiple oligodendrocytes in close proximity to the neuron soma in the "cloud"; (B) Photomicrograph of the cloud (detail of D) showing the network of thick myelinated fibers; (C & D) low magnification image of Nissl (C) and Luxol Fast Blue (D) staining. (E) Photomicrograph (detail of C) showing that neuron soma are more concentrated than in the "cloud" (A); (F) Photomicrograph (detail of D) showing that myelinated fibers are less concentrated than in the "cloud" (B); Scale bars: A, B, E, F = 10 μm; C, D = 1 mm.

Figure 8. Histological characterization of the extreme and external capsules. Photomicrographs of a Nissl (A) and Luxol Fast Blue (B) stained sections displaying the boundary (black lines) between the claustrum and the capsules. Cl, claustrum; ex, external capsule; ext, extreme capsule; ic, insular cortex. Scale bars = 100 μm.

Figure 9. Silhouette plot showing how soma size and shape form 2 unique and tightly grouped clusters with very few outliers. Within each cluster, the high silhouette values suggest that the objects are well-matched.
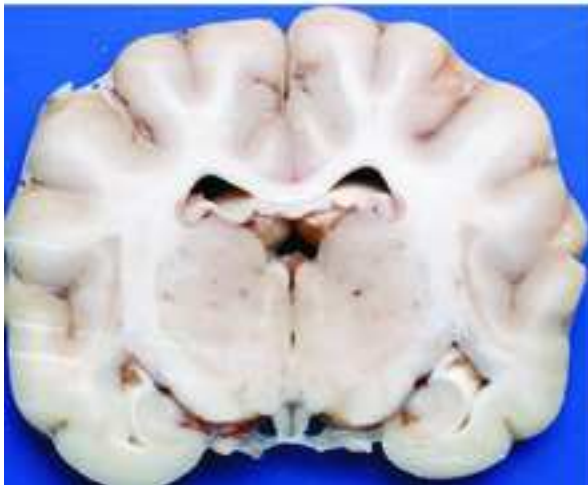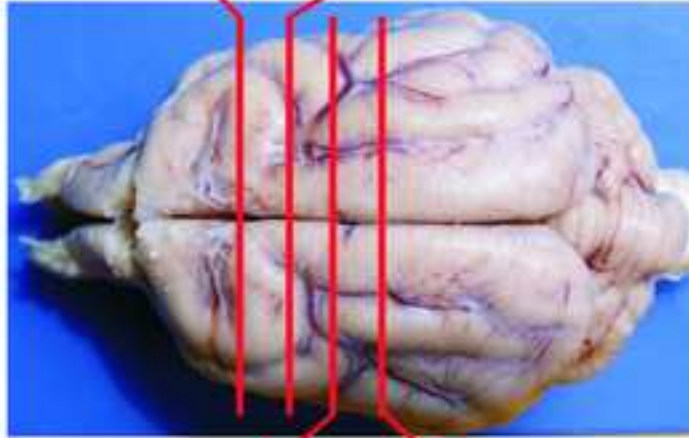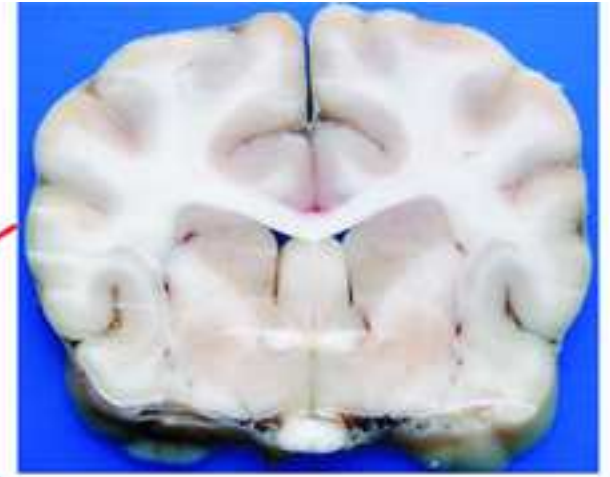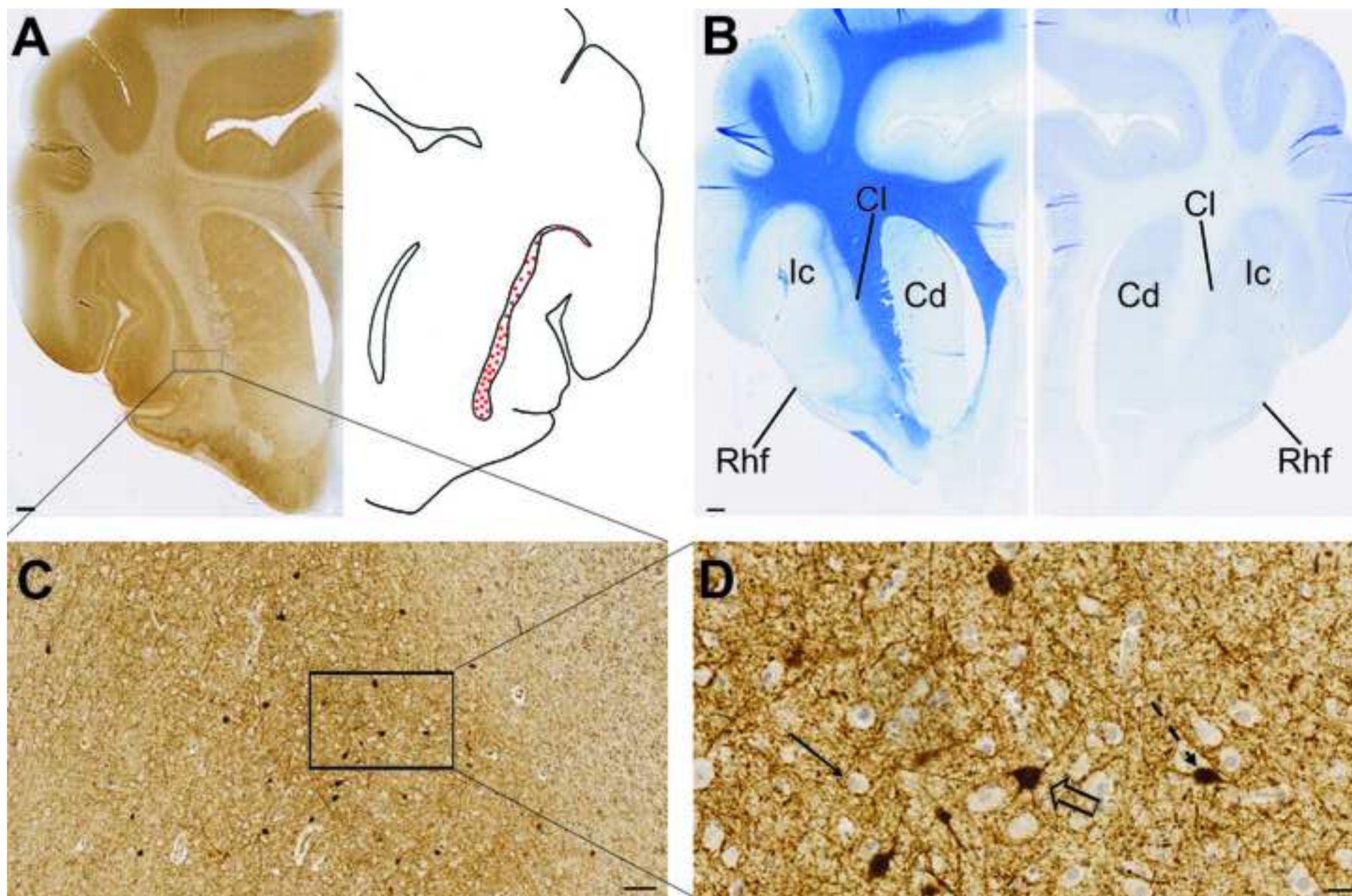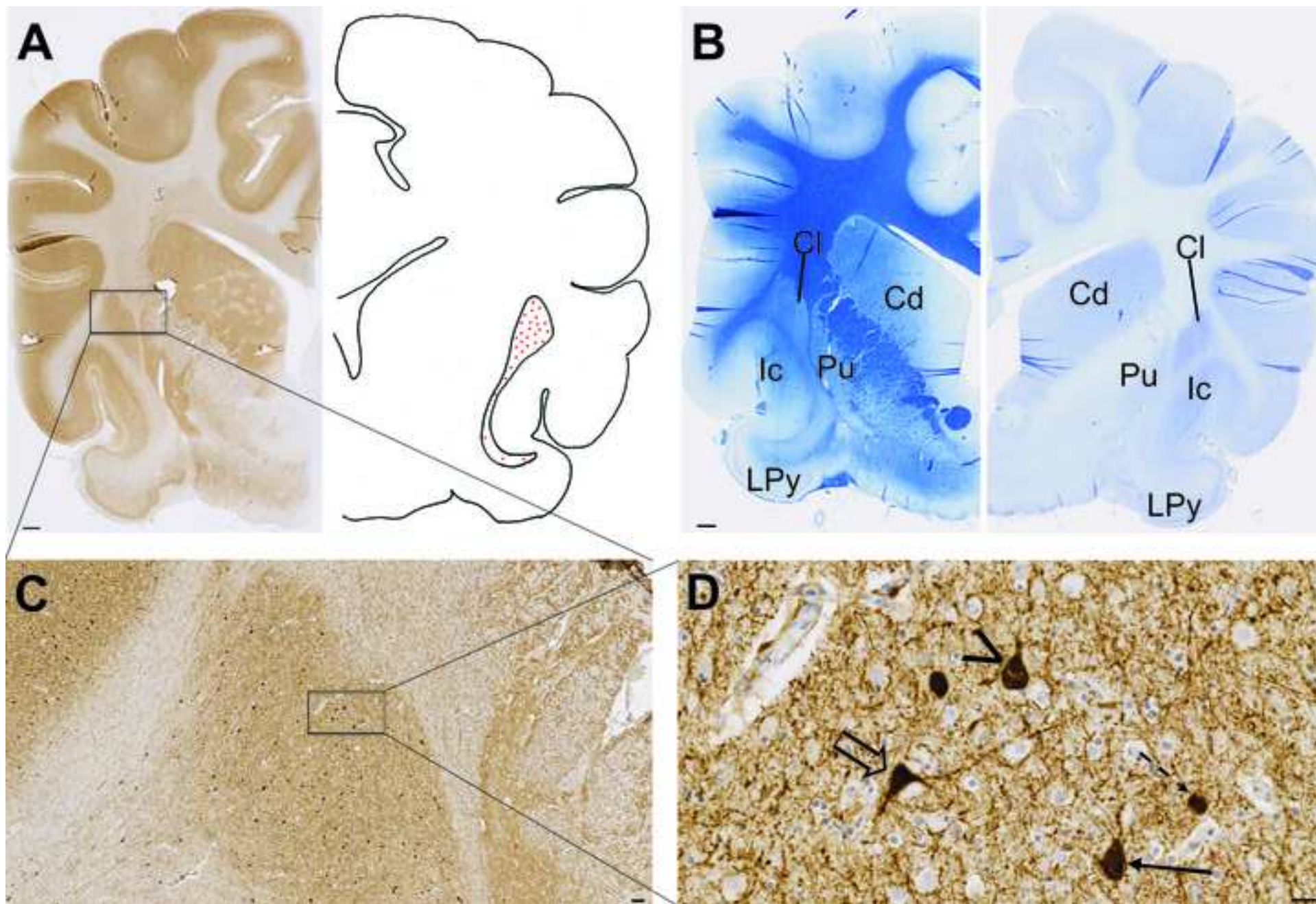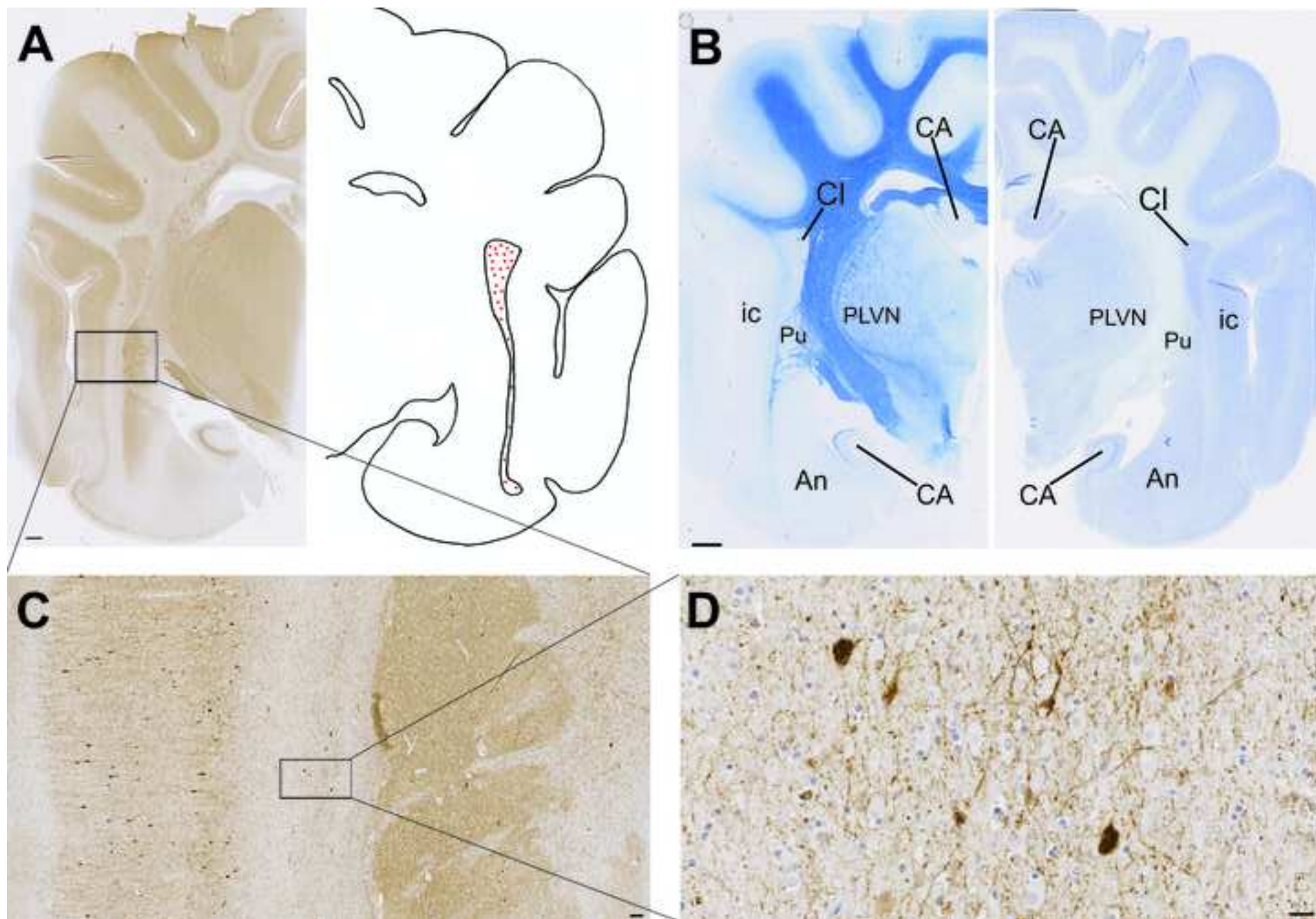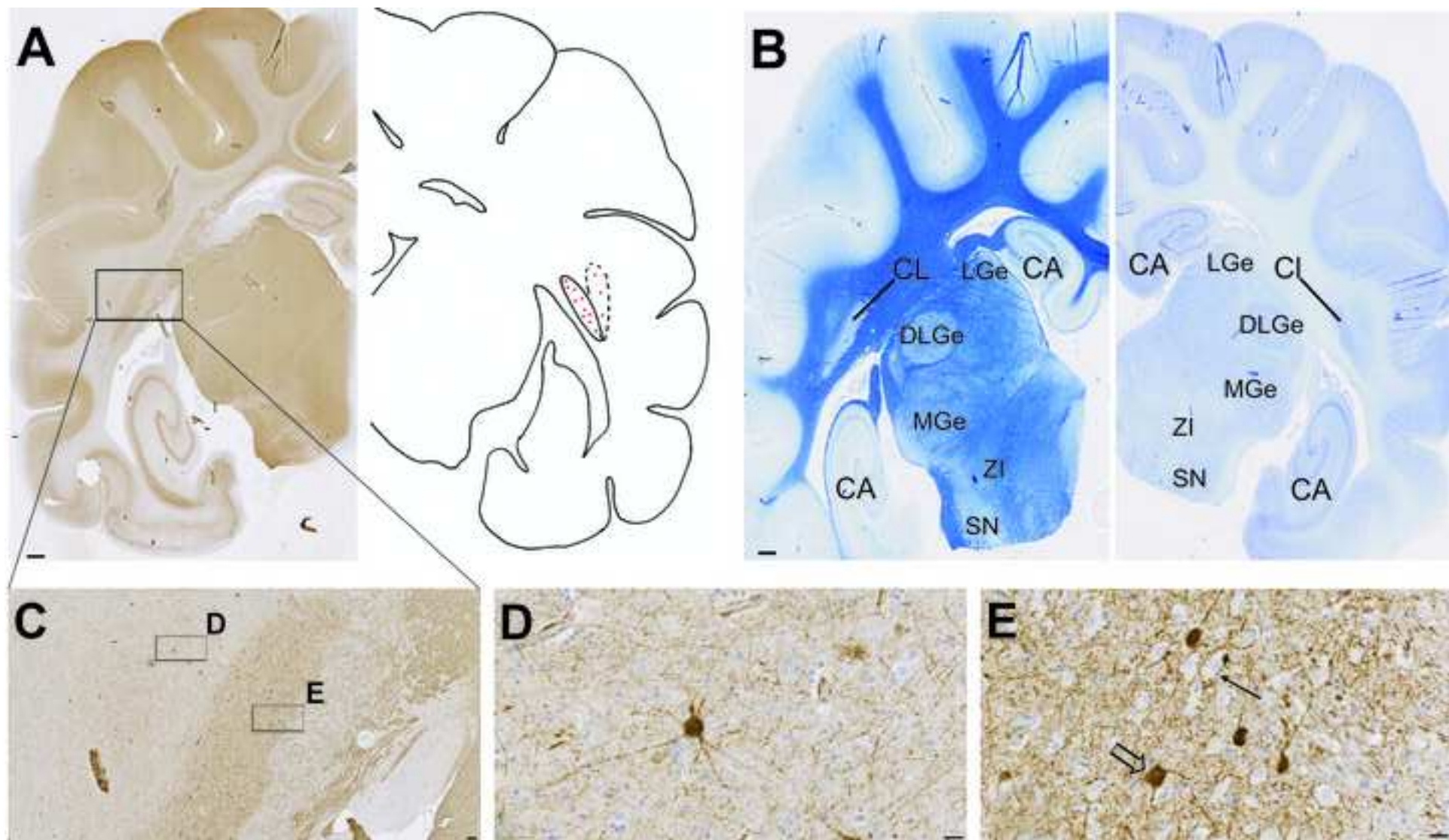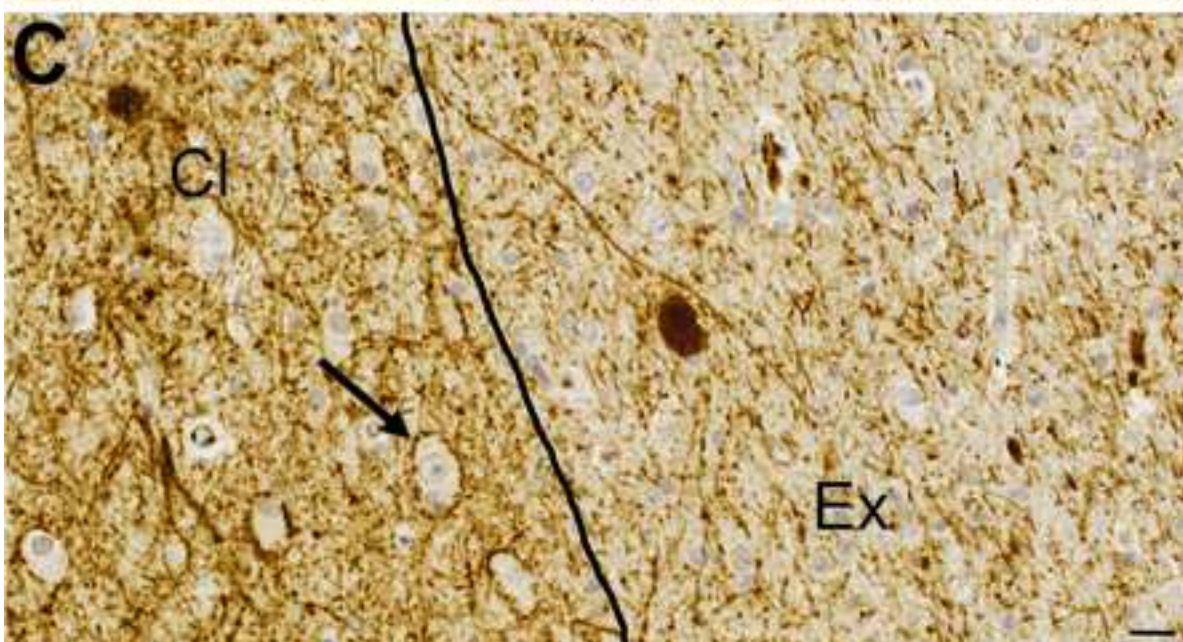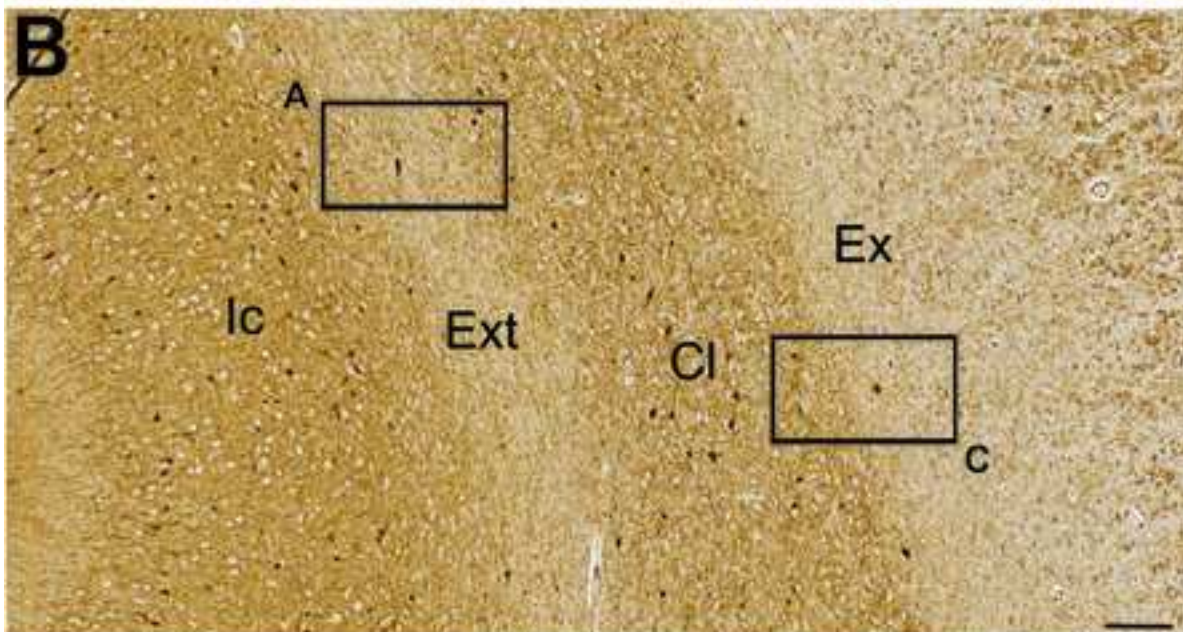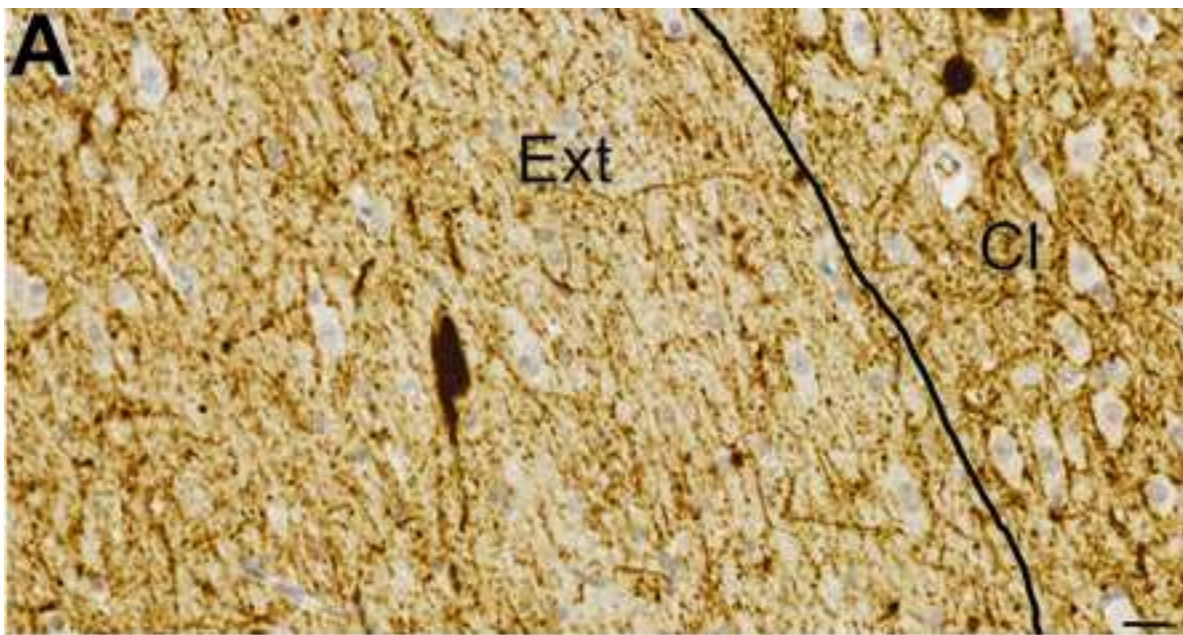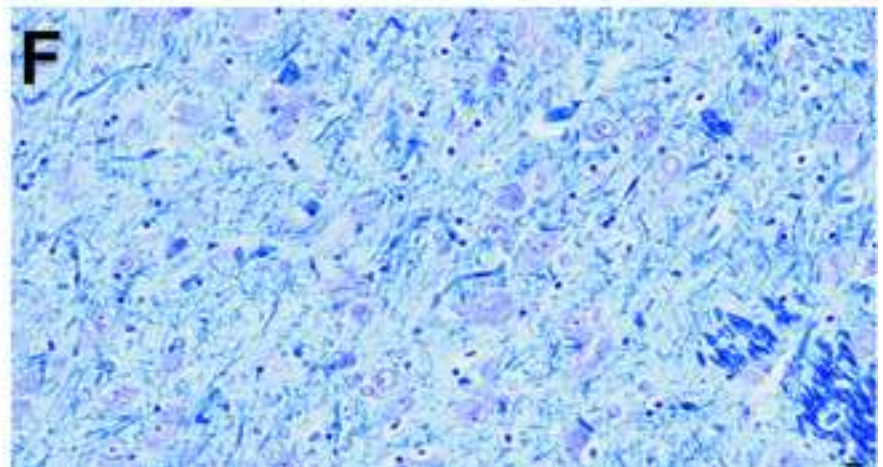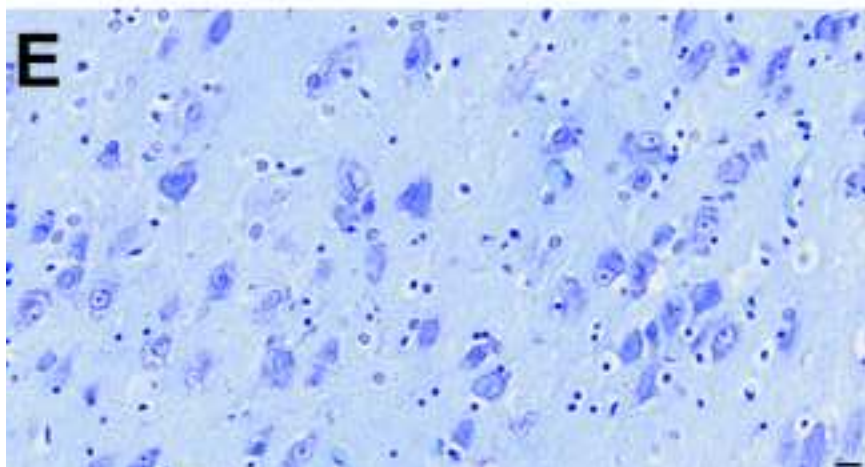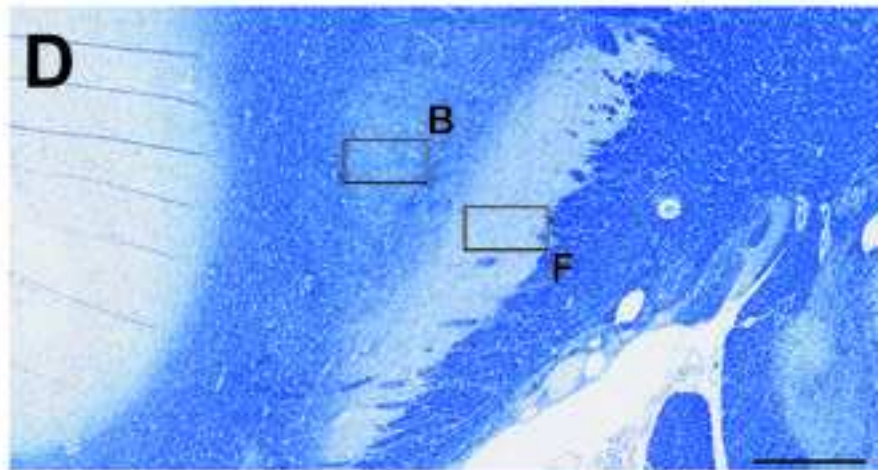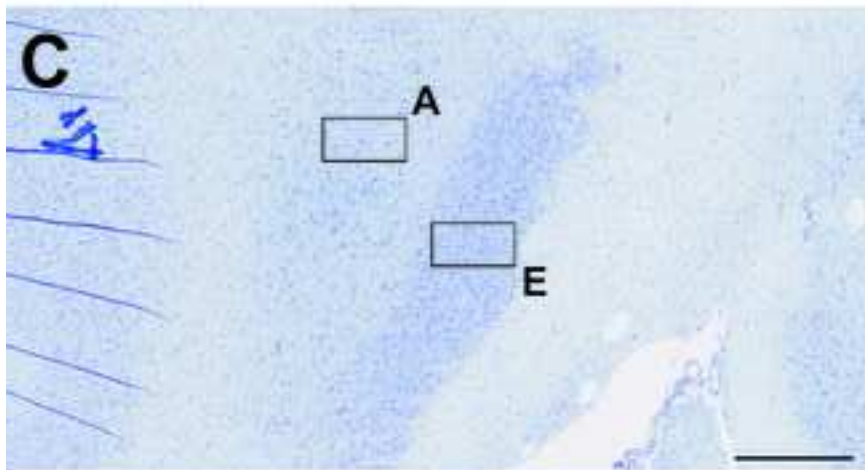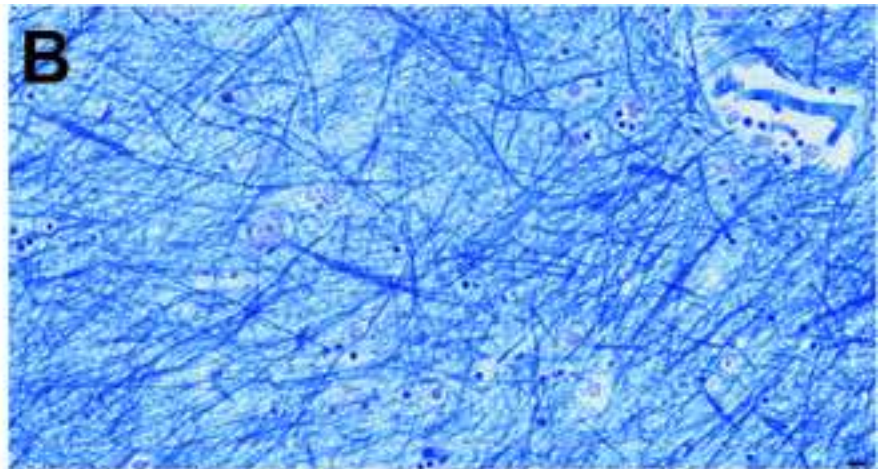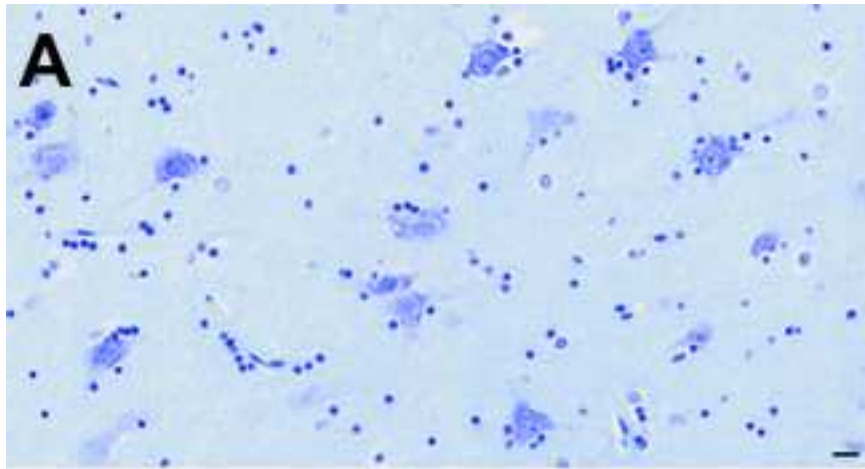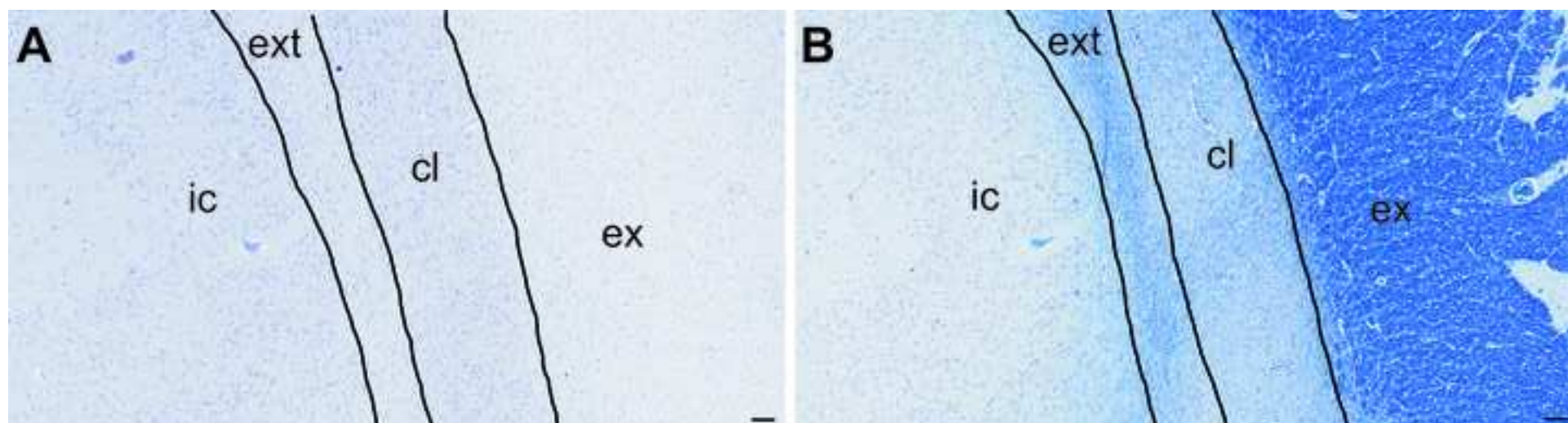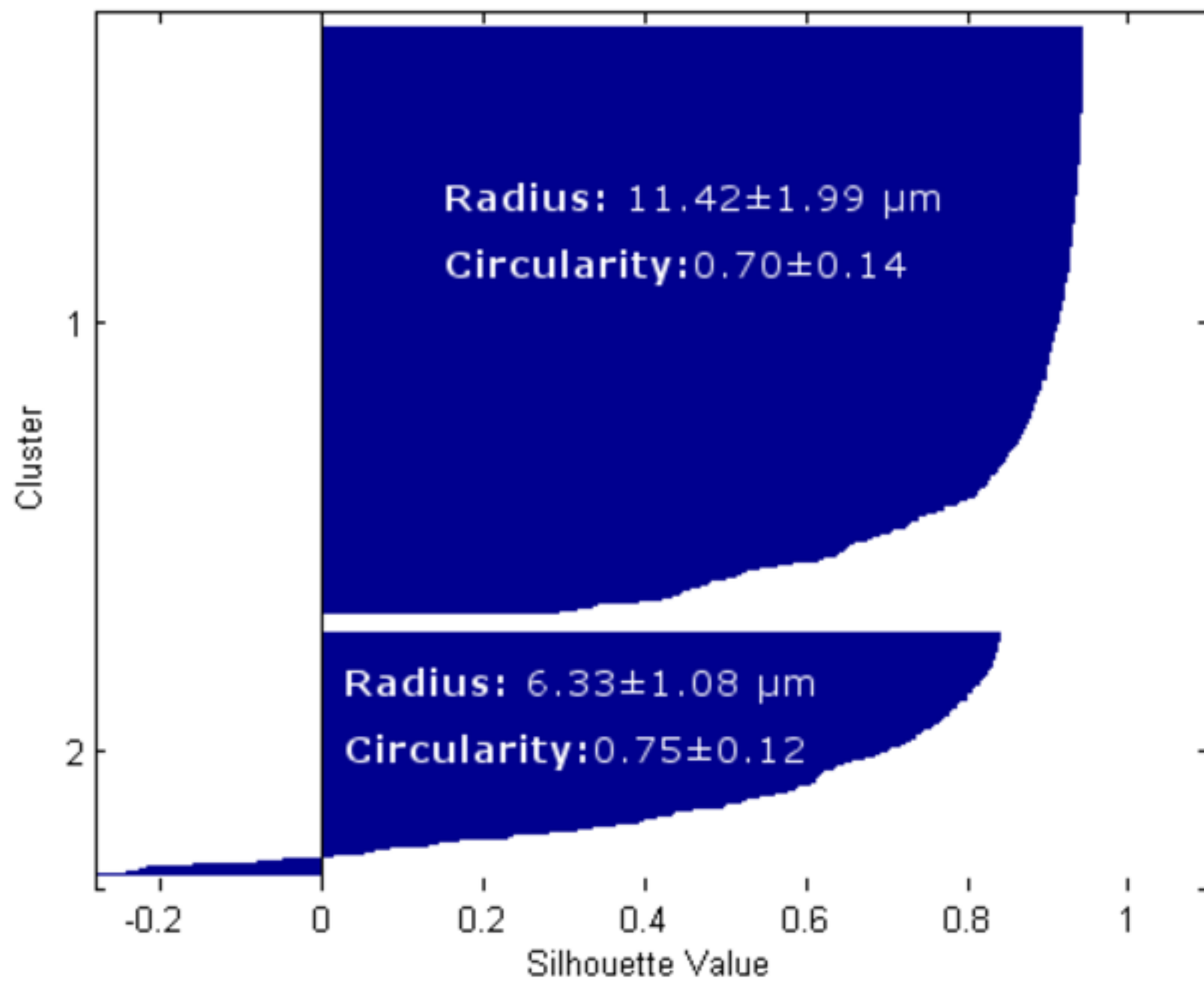
David H. Reser

Department of Physiology, Monash University

Clayton, Bldg. 13F, Clayton, VIC 3800, Australia

e-mail: david.reser@monash.edu

Bruno Cozzi

Department of Comparative Biomedicine and Food Science University of Padova

Viale dell'Università, 16, 35030 Legnaro - Agripolis (PD) ITALY

e-mail : bruno.cozzi@unipd.it

Dear Editor,

Since archival samples were used, Institutional Animal Care and Use Committee approval was not required. Use of archival samples is encouraged by the EU Directive 2010/63/ of 22 September 2010 on the protection of animals used for scientific purposes.

There is no conflict of interest including any financial, personal or other relationships with other people or organizations that could inappropriately influence, or be perceived to influence this work.

The work described has not been published previously.

All authors have materially participated in the research or in the article preparation.

Yours sincerely,

Andrea Pirone, Ph.D.
Department of Veterinary Sciences
University of Pisa
viale delle Piagge 2
56124 Pisa
ITALY
phone + 39.050.2216808
e-mail <apirone@vet.unipi.it>